where Γ and ζ are the Riemann Γ function and the ζ function, respectively.
14. Y. Rephaeli, M. Ulmer, D. Gruber, *Astrophys. J.* **429**, 554 (1994).
15. R. J. Hanisch, *Astron. J.* **85**, 1565 (1980).
16. ———, R. G. Strom, W. J. Jaffe, *Astron. Astrophys.* **153**, 9 (1985).
17. K.-T. Kim, P. P. Kronberg, G. Giovannini, T. Venturi, *Nature* **341**, 720 (1989).
18. G. Giovannini, L. Feretti, T. Venturi, K.-T. Kim, P. P. Kronberg, *Astrophys. J.* **406**, 399 (1993).
19. L. Feretti, D. Dallacasa, G. Giovannini, A. Tagliani, *Astron. Astrophys.* **302**, 680 (1995).
20. R. Mewe, E. H. B. M. Gronenschild, G. H. J. van den Oord, *Astron. Astrophys. Suppl. Ser.* **62**, 197 (1985).
21. D. E. Harris and J. E. Grindlay, *Mon. Not. R. Astron. Soc.* **188**, 25 (1979).
22. D. E. Harris, in *Low Frequency Astrophysics from Space*, N. E. Kassim and K. W. Weiler, Eds. (Lecture Notes in Physics no. 362, Springer-Verlag, Berlin, 1990), pp. 252–261.
23. V. S. Ptuskin, in *Astrophysics of Cosmic Rays*, V. L. Ginzburg, Ed. (Elsevier, Amsterdam, 1990), pp. 171–215.
24. B. Dennison, *Astrophys. J.* **236**, 761 (1980).
25. J. P. Vallee, *Astron. J.* **99**, 459 (1990).
26. I thank D. E. Harris, S. Bowyer, R. Lieu, L.-W. Chen, and K. Y. Lo for useful discussions and comments. I also acknowledge support from Academia Sinica and the National Science Council of the Republic of China in Taiwan.

8 July 1997; accepted 30 October 1997

A Pulsar, the Heliosphere, and Pioneer 10: Probable Mimicking of a Planet of PSR B1257+12 by Solar Rotation

Klaus Scherer,*† Horst Fichtner, John D. Anderson, Eunice L. Lau

Doppler data generated with the Pioneer 10 spacecraft's radio carrier wave between 1987 and 1995 show a 25.3-day periodicity which is related to the solar rotation. The timing data of the pulsar PSR B1257+12 also show a periodicity of 25.34 days, which has been explained as a signature of the pulsar's barycentric motion in response to the existence of a small moon-like object. However, because PSR B1257+12 is located close to the ecliptic and because the timing variations are in the range of microseconds, it is likely that the pulsar signal is affected by the same mechanism acting on the Pioneer 10 Doppler data. Hence, the hypothesized inner planet around PSR B1257+12 is probably an artifact of the heliosphere.

Variations in the timing data of the pulsar PSR B1257+12 with periodicities of 25.34, 66.54, and 98.22 days have been explained by its motion around the barycenter, defined by the pulsar and three hypothesized planets (*1*). In fitting these data, multibody simulations were used to describe the planetary evolution over tens of years (*2*), and, with a vectorial integration method (*3*), it has been shown that the three-planet system would be stable over some hundreds of thousands of years.

Despite this plausible explanation of the timing data, the three-planet hypothesis has to be checked against other interpretations. In particular, as has been demonstrated (*4*) in connection with the suspected extrasolar planet around 51 Pegasi, serious consideration has to be given to the question of whether the planets are real. In light of this, we demonstrate that the innermost moon-like planet around PSR B1257+12 probably does not exist.

We base this hypothesis on the dominant period in the Pioneer 10 (P10) radio Doppler data (*5*) of 25.3 days, which is indistinguishable from the suspected revolution period of the inner planet around PSR B1257+12. The P10 Doppler data are obtained by a "two-way radio link" experiment, where a signal with a frequency f = 2.1 GHz is transmitted from Earth (uplink), transponded by the spacecraft, and hours later is received back at Earth (downlink). With a local oscillator (a highly stable hydrogen maser), it is possible to determine the Doppler shift to an accuracy of better than 1 mHz (*6*). After removing systematic changes in the position and velocity of P10 caused by the motion of the planets and the moon, periods of 13.3 days (*7*), 25.3 days (Fig. 1), and about 1 year (Fig. 2) (*8*) remained. The periods cannot be produced as a result of an acceleration of the spacecraft by the ram pressure of the solar wind ($a_{ram} \approx 5 \times 10^{-17}$ km s^{-2}) or by the solar radiation pressure ($a_{rad} \approx 5 \times 10^{-15}$ km s^{-2}), because their contribution is orders of magnitude smaller than the standard error in the reduced Doppler data.

To test the idea that the solar wind patterns are responsible for these P10 periodicities, we calculated the autocorrelation of the reduced Doppler data (Figs. 2 and 3) and compared it with the cross-correlation of the Doppler data with the solar wind proton density recorded by P10, by Voyager 2 (V2) (Fig. 2), and by the Interplanetary Monitoring Platform (IMP) (*9*) spacecraft (Fig. 3). The cross-correlation functions have a shape similar to that of the autocorrelation function (Fig. 2). The relative shift between the two cross-correlation functions can be explained by the different heliocentric distances (r) and ecliptic latitudes (β) and longitudes (λ) of P10 and V2. Although the cross-correlation is performed using the observed proton density data, the result is valid for the unobserved electron density too, because of the quasi-neutrality of the solar wind. In addition to the P10 and V2 plasma data, we correlated the reduced Doppler data with the plasma data obtained by the IMP spacecraft at 1 astronomical unit (AU) (Fig. 3). In this case, the auto- and cross-correlation functions have different shapes for larger time lags, but are very similar to each other for short time lags.

To determine any periodicities shorter than 1 year, we applied the maximum entropy method to a 9-month (*10*) coherent raw Doppler data set (Fig. 1) in 1993. The data show two periods of 25.3 and 13.3 days at a confidence level >95% and periods of 52.9, 18.5, and 11.2 days at a confidence level >50%. Here, we are interested only in the 25.3-day period, which can be explained as follows: In the ecliptic plane, the radio wave propagates through the interplanetary medium, which is not uniform but resembles the rotation of the sun, especially the structured patterns induced by the sector struc-

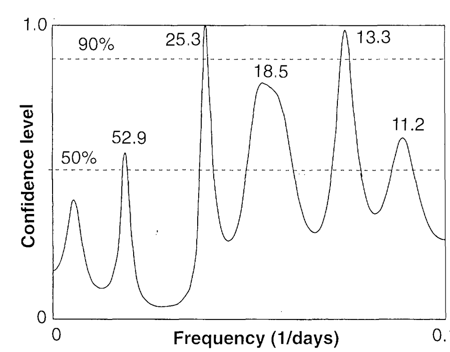

Fig. 1. Periodogram calculated by the maximum entropy (all poles) method for reduced P10 Doppler data over an interval of about 9 months centered on solar opposition.

K. Scherer, J. D. Anderson, E. L. Lau, Jet Propulsion Laboratory, Mail Stop 301/230, Pasadena, CA 91119, USA.
H. Fichtner, Institut für Astrophysik und Extraterrestrische Forschung der Universität Bonn, Auf dem Hügel 71, D-53121 Bonn, Germany.

*To whom correspondence should be addressed. E-mail: scherer@lindust.mpae.gwdg.de
†Present address: Max-Planck-Institut für Aeronomie, D-37191 Katlenburg-Lindau, Germany.

ture of the solar wind. The 1-year period, as well as the shorter periods, are caused by the spatially changing solar wind patterns, which look like explicit time variations of the electron density along the line of sight through the heliosphere. Such variations of the solar wind plasma parameters with a period equal to or close to the half and full (sidereal) solar rotation period are typical and are seen in many observations connected with so-called corotating interaction regions [CIRs (*11*)] formed at low- to midheliocentric latitudes (within $\approx\pm 40°$). These periodicities were observed by P10 at distances between 40 AU and 65 AU from 1987 to 1997. The pulsar PSR B1257+12 and P10 are at low heliocentric latitude ($\beta \approx 17°$ and $\beta \approx -3°$) and hence have a similar ray path inside the heliosphere. Therefore, the 25.34-day period of PSR B1257+12 may be caused by the solar wind plasma, like the 25.3-day period of P10, rather than being associated with an orbiting satellite around the pulsar.

The 25.34-day period of the variations of the pulsar pulse data is close to the rotation period of the sun (25.2 days at 10°, 25.6 days at 20°) at 17°. Therefore, the pulsar's timing data should be affected by the same mechanism responsible for the variations in the P10 radio data, because variations in the electron density are expected for all low- and midheliographic latitudes. Also, for the time span in 1993 where the 25.34-day variation has been seen directly in the data, an electron density variation with solar rotation was deduced with the Ulysses spacecraft (*11*).

The amplitude of the variation in time of arrival (TOA) of the pulsar signal caused by temporal changes of heliospheric electron density (*12*) can be calculated from

$$\mathrm{TOA} = \int^{l} \frac{dl}{v} \approx \int^{l} \left[1 + \frac{1}{2}\left(\frac{f_{\mathrm{p}}}{f}\right)^{2}\right] \frac{dl}{c} = \frac{l}{c} + \frac{40.31}{c}\frac{1}{f^{2}} \int^{l} N_{\mathrm{e}} ds = \frac{l}{c} + \Delta T \qquad (1)$$

where f_{p} is the plasma frequency, f is the frequency of the radio wave, N_{e} is the electron number density along the line of sight l, c is the speed of light, and v is the group velocity of the radio wave. The first part of the right-hand side in Eq. 1 describes the classical Doppler effect, while the second part (ΔT) is the dispersion of the radio signal due to the electron column density.

The variations in the TOA can be interpreted in two ways: (i) The distance of the pulsar varies periodically because of the motion of the barycenter, or (ii) the electron density along the ray path varies because of the corotating patterns of the solar wind. In the first case, the barycentric ellipse of the pulsar caused by the innermost planet has a semimajor axis less than 1 km (*13*). In the second case, we find from the IMP spacecraft that average proton number density of the solar wind changes quasi-periodically about $\overline{N}_{\mathrm{e}}$(1 AU) $\approx$ 8 cm^{-3} with an amplitude up to 6 cm^{-3}, that is, N_{e}(1 AU) = (8 ± 6) cm^{-3}. Although this is an oversimplified model of the spatial solar wind variability, it is sufficient to give a lower limit for the magnitude of the TOA variations. Despite a corotating spiral pattern in the overall electron density connected with CIRs at low and midlatitudes, $\overline{N}_{\mathrm{e}}$ decreases with r^{-2}, so only the lower boundary of the integral contributes significantly to the TOA. At the upper boundary (the outer boundary of the heliosphere), which is of the order of ~100 AU, the electron number density is about four orders of magnitude smaller. Another indication that the inner heliospheric electron distribution is mainly responsible for the variations is given by the fact that the variation of the P10 Doppler data also exhibits a period of about half the solar rotation period. This period is typical for plasma variations in the inner heliosphere (*7*).

Evaluating the dispersive Doppler effect ΔT for an inner boundary of 1 AU and the two frequencies f = 430 and 1400 MHz at which the pulsar has been observed (*1*), we find ΔT_{430} = (0.21 − 1.51)μs and ΔT_{1430} = (0.02 − 0.15)μs. Obviously, the modulation of the pulsar pulses as a consequence of the varying heliospheric electron density is in the microsecond range where the TOA variations attributed to a third planet are observed. These estimates are lower limits because the integral in Eq. 1 was evaluated for the opposition configuration. For all other relative positions of sun, Earth, and PSR B1257+12, the electron contents along the line of sight is higher because the latter passes through a region of higher electron density (*14*).

In addition to our conclusion that the hypothesized innermost body around PSR B1257+12 is not real and, therefore, only two planet-like objects (*15*) are orbiting the pulsar, we would like to point out that our study suggests that TOA data of pulsar pulses provide a useful technique to probe the three-dimensional plasma structure in the low- to mid-latitude heliosphere. A similar technique has been used since 1981 to probe the solar corona (*16*). A

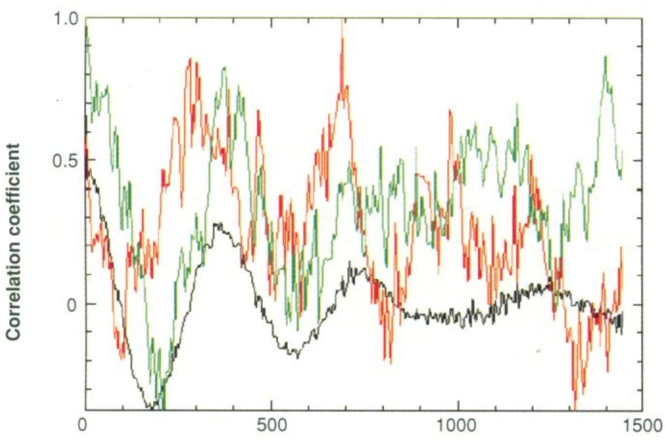

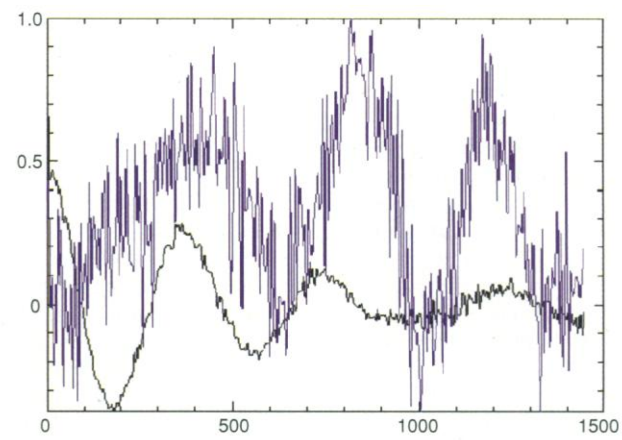

Fig. 2 (left). The black curve shows the real part of the autocorrelation function of the P10 Doppler data. The red and green curves are the cross-correlation between the P10 Doppler data and the proton density recorded by P10 and V2, respectively. The imaginary parts of all three functions are negligible compared to the real parts. The two cross-correlation functions are very similar in shape to the autocorrelation function, indicating that all three functions show the same periodicity. **Fig. 3 (right).** The solid curve is the autocorrelation of the P10 Doppler data, while the blue curve is their cross-correlation with the solar wind proton density monitored on the IMP spacecraft orbiting Earth.

continuous monitoring of the heliosphere with ground-based radio telescopes could substantially supplement future spacecraft observations, thus suggesting a future synergistic approach to ground- and space-based observations.

REFERENCES AND NOTES

1. A. Wolszczan, *Science* **264**, 538 (1994).
2. R. Malhotra, *Astrophys. J.* **407**, 266 (1993); F. A. Rasio, P. D. Nicholson, S. L. Shapiro, S. A. Teukolsky, in *Planets Around Pulsars*, J. A. Phillips, J. E. Thorsett, S. R. Kulkarni, Eds. (ASP Conf. Ser. 36, Astronomical Society of the Pacific, San Francisco, CA, 1993), pp. 107–119.
3. K. Scherer and J. D. Anderson, *Eos (Fall Suppl.)* **76**, F332 (1995).
4. D. F. Gray, *Nature* **385**, 795 (1997).
5. The experiment was designed as a celestial mechanics experiment to measure masses, special relativity effects, and recently, to detect large objects in the Edgeworth-Kuiper Belt.
6. The Doppler data are coherently referenced to hydrogen-maser frequency standards at Deep Space Network (DSN) stations in California, Australia, and Spain, and the radio wave transmitted from the ground is transponded by the spacecraft's telecommunication subsystem with a frequency ratio of 240/221. A summary of the Pioneer telecommunication subsystem, as well as other aspects of the spacecraft and its mission, can be found in R. O. Fimmel, J. Van Allen, and E. Burgess [*Pioneer: First to Jupiter, Saturn, and Beyond*, NASA SP-446 (Government Printing Office, Washington, DC, 1980)]. For a discussion of nonlinear least squares applied specifically to spacecraft orbit determination, see T. D. Moyer [*Mathematical Formulation of the Double Precision Orbit Determination Program* (JPL TR 32-1527, Jet Propulsion Laboratory, Pasadena, CA, 1971)], B. D. Tapley [in *Recent Advances in Dynamical Astronomy*, B. D. Tapley and V. Szebehely, Eds. (Reidel, Boston, MA, 1973), pp. 396–425], and J. D. Anderson [in *Experimental Gravitation*, B. Bertotti, Ed. (Academic Press, New York, 1974), pp. 163–199].
7. K. Mursula and B. J. Zieger, *J. Geophys. Res.* **101**, 27077 (1996).
8. J. D. Richardson, K. I. Paularena, J. W. Belcher, A. J. Lazarus, *Geophys. Res. Lett.* **21**, 1559 (1994).
9. The solar wind data can be found at the following Web sites. Ames Research Center Pioneer Plasma Group home page: http://arwen.arc.nasa.gov; National Space Science Data Center (NSSDC) COHOWeb: http://nssdc.gsfc.nasa.gov/cohoweb/form/cw_ds.html; NSSDC OMNIWeb: http://nssdc.gsfc.nasa.gov/omniweb/ow.html
10. The data do not cover a full year because during conjunction the radio ray path passes the sun at about 11 solar radii, which is very close to the formation region of the solar wind in the ecliptic. Therefore turbulent plasma processes are dominant, and the radio signal to P10 is noisy.
11. R. von Steiger, J. Geiss, G. Gloeckler, A. B. Galvin, *Space. Sci. Rev.* **72**, 71 (1995); L. F. Burlaga, *J. Geophys. Res.* **93**, 4103 (1988); J. L. Philips *et al.*, *Science* **268**, 1030 (1995).
12. M. K. Bird, *Space. Sci. Rev.* **33**, 99 (1982).
13. With a pulsar mass m_{PSR} of 1.4 solar masses, a planetary mass m_C of 0.015 Earth masses, and the planetary semimajor axis a_C = 0.19 AU, it follows from $a_{PSR} = a_C m_C / m_{PSR}$ = 0.19 km.
14. D. O. Muhleman and J. D. Anderson, *Astrophys. J.* **247**, 1093 (1981).
15. A possible third object with a revolution period of about 170 years was recently reported [A. Wolszczan, in *Pulsars: Problems and Progress*, M. Bailes, S. Johnston, M. Walker, Eds., *IAU Colloquium* **160**, 91 (1996)].
16. M. K. Bird, in *Solar Wind 4*, H. Rosenbauer, Ed. (*Report MPAE-W-100-81-31*, Max-Planck-Insitut für Aeronomie, Katlenburg-Lindau, Germany, 1981), pp. 78–83.

17. Part of this work was sponsored by the Pioneer Project, NASA Ames Research Center and was performed at the Jet Propulsion Laboratory (JPL), California Institute of Technology, under contract with NASA. The Pioneer 10 radio Doppler data were generated with the support of JPL's Telecommunications and Mission Operations Directorate and the DSN.

14 August 1997; accepted 30 October 1997

Radar Detection of the Nucleus and Coma of Comet Hyakutake (C/1996 B2)

J. K. Harmon,* S. J. Ostro, L. A. M. Benner, K. D. Rosema, R. F. Jurgens, R. Winkler, D. K. Yeomans, D. Choate, R. Cormier, J. D. Giorgini, D. L. Mitchell,† P. W. Chodas, R. Rose, D. Kelley, M. A. Slade, M. L. Thomas

Radar observations of comet Hyakutake (C/1996 B2) made at the Goldstone Deep Space Communications Complex in California have detected echoes from the nucleus and from large grains in the inner coma. The nucleus of this bright comet was estimated to be only 2 to 3 kilometers in diameter. Models of the coma echo indicate backscatter from porous, centimeter-size grains ejected anisotropically at velocities of tens of meters per second. The radar observations suggest that a comet's activity may be a poor indicator of its size and provide evidence that large grains constitute an important component of the mass loss from a typical active comet.

Radar is one of the most powerful Earth-based techniques for studying comets because it can be used to directly probe the nucleus as well as identify populations of large grains in the coma. Unfortunately, comet radar detections are rare events, because few of these small objects pass close enough to Earth to give measurable echoes. Before Hyakutake only five comets had yielded radar detections. Three of these detections [P/Encke (*1*), P/Grigg-Skjellerup (*2*), and C/Sugano-Saigusa-Fujikawa 1983 J1 (*3*)] were of the nucleus alone. Comet C/IRAS-Araki-Alcock 1983 H1 (henceforth referred to as IAA) made the closest approach [0.031 astronomical unit (AU)] of the five and also was the first to show echoes from large coma grains as well as from the nucleus (*4*, *5*). The 1985 apparition of comet P/Halley produced the last and most distant (0.63 AU) comet radar detection; Halley showed only a coma echo, the nucleus echo being too weak to be seen at this distance (*6*). Comet Hyakutake (C/1996 B2), which passed within 0.10 AU of Earth, offered the first good comet radar opportunity in 13 years and the first chance to observe a bright comet at close range.

J. K. Harmon, National Astronomy and Ionosphere Center, Arecibo Observatory, Post Office Box 995, Arecibo, PR 00614, USA.
S. J. Ostro, L. A. M. Benner, K. D. Rosema, R. F. Jurgens, R. Winkler, D. K. Yeomans, D. Choate, R. Cormier, J. D. Giorgini, D. L. Mitchell, P. W. Chodas, R. Rose, D. Kelley, M. A. Slade, M. L. Thomas, Jet Propulsion Laboratory, California Institute of Technology, 4800 Oak Grove Drive, Pasadena, CA 91109-8099, USA.

*To whom correspondence should be addressed.
†Present address: Space Sciences Laboratory, University of California, Berkeley, CA 94720, USA.

Radar observations of Hyakutake were made in March 1996 with the X-band (8510 MHz; wavelength, λ, of 3.5 cm) radar on the 70-m antenna at the Goldstone facility in California. Echo detections were obtained on 24 and 25 March, when the comet was near its closest approach distance (Fig. 1). As with previous comet detections, the Hyakutake detections were made with an unmodulated continuous-wave (CW) transmission (*7*). A 490-kW, circularly polarized wave was transmitted, and the echoes were received in the opposite-sense circular (OC) and same-sense circular (SC) polarizations (*8*). The received signal was sampled and analyzed to give calibrated (*9*) echo power spectra with frequency resolutions of either 19.5 Hz (low resolution) or 1.95 Hz (high resolution). The spectra were summed for each polarization to give one low-resolution and one high-resolution spectrum pair for 24 March, and one low-resolution spectrum pair for 25 March.

Both low-resolution spectra (Fig. 2, A and B) from the two successive days show a narrow spike, which is the nucleus echo, along with a broad hump skewed toward the negative side of the spike, which is the coma echo. The nucleus echo can also be seen at 210 Hz in the high-resolution spectrum (Fig. 2C). (The total bandwidth of this spectrum was too narrow to recover the full coma echo, and we have subtracted any residual coma echo left after noise baseline removal.) Integrating under the three nucleus echoes in Fig. 2 gives total radar cross